Study of Polymer Melt Flow in Sequential Injection Molding Process

S. C. Chen, N. T. Chen, K. S. Hsu, and K. F. Hsu
Mechanical Engineering Dept., Chung Yuan University, Chung-Li, Taiwan 32023, ROC

Experimental studies of polymer melt flow in the filling and post-filling stages of the injection molding process were performed using the sequential injection of transparent and colored polystyrene resin. Effects of fountain flow in the filling stage, geometrical factors caused by edges and corners, as well as flow through contractions and expansions, were identified. Significant polymer melt flow which increases with increased packing pressure was observed in the post-filling process. The melt flow is more concentrated around the gate area than away from the gate. It was also found that the polymer melt flows across the gap center, resulting in partial annihilation of the weld line. Simulations based on the control-volume/finite-element method employed within each gapwise layer combined with the dual-filling-parameter technique were developed to trace the advancements in melt fronts for both skin and core materials. Numerical simulations show reasonable consistency with experimental results in both skin and core material distribution. If the edge effect is taken into account using a shape factor as a geometrical correction, the simulation accuracy is further improved.

Introduction

Injection molding, being a versatile operation for the mass production of complex plastics parts, is one of the most widely employed methods of polymer processing. The injection molding process consists of three major stages including filling, packing, and cooling. In the filling stage, hot molten polymer is injected into the mold cavity. Once the cavity is filled, additional polymer melt is forced into the cavity under high pressure in order to compensate for the subsequent shrinkage due to the solidification.

As a result of the extensive application of plastics in all areas of industry, there is not only an increasing need for injection molds, but also a strong request of high quality parts with special features normally unavailable by means of conventional molding methods. Recently, innovative injection molding processes have been developed for this purpose. Coinjection molding (also named as sandwich molding) is one such innovative molding technique. In the coinjection molding process, a skin polymer melt and a dissimilar but compatible core polymer melt were simultaneously or sequentially injected into a mold cavity so that the core material was embedded within the solidified layers of the skin material (Escales, 1970; Eckardt, 1985, 1986; Kreisher, 1990). This process was originally designed to provide flexibility in part design and manufacture by utilizing the optimal properties of each material. For example, low-cost or recycled plastics can be used as core material sandwiched within thin, expensive, rigid skin plastics, or skin material can be used with formed core material to reduce part weight and part residual stress. Generally speaking, if the coinjection molding process is properly designed, part weight, part cost, injection pressure, residual stress, and warpage can be reduced and the modification of part properties can also be achieved. On the other hand, when a transparent skin material and a colored core material of the same brand are used, flow information may be obtained directly by viewing the coinjection molded parts. To perform a more rigorous investigation on polymer melt flow, sequential injection, one of the capabilities of the coinjection molding technique, can be utilized. The sequential injection molding process is illustrated in Figure 1.

Visualization techniques of polymer melt flow have been developed to study molding dynamics (Schmidt, 1974; Coyle et al., 1987; Vos et al., 1991; Yokoi et al., 1991, 1992). Schmidt first applied a tracer technique in the injection molding process to observe fountain flow. Around the melt front re-

Correspondence concerning this article should be addressed to S. C. Chen.

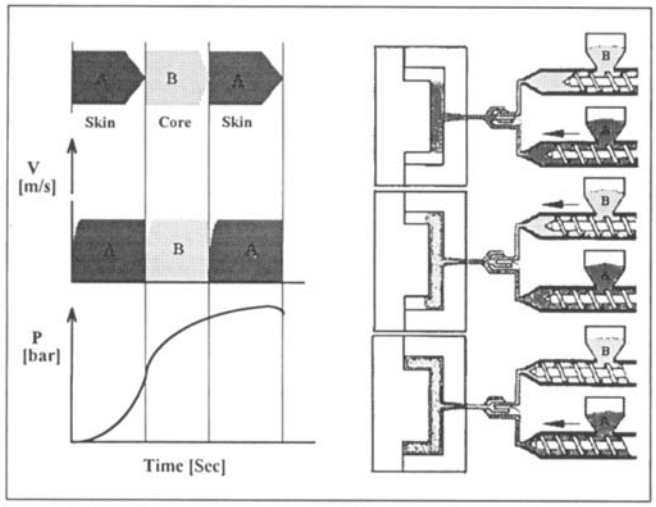

Figure 1. Sequential injection molding process.

gion, polymer melt decelerates in the direction of flow and acquires a transverse velocity, spilling outward from melt core toward the cavity wall. This is known as the fountain flow effect. Later on, Coyle et al. (1987) and Vos et al. (1991) experimentally investigated the flow field near the fountain flow region in more detail. Among these methods, visualization with laser light or high-speed video camera in a glass-inserted mold has recently been used by Yokoi et al. (1991, 1992). Although the dynamic visualization technique using a transparent mold can investigate time-sequential molding phenomena for the thick cavities in detail, it is also subject to the limitations of the maximum allowable injection pressure, the limited observation area, as well as the complexity and the expense in mold construction. Therefore, it is difficult to apply such a technique to thin cavities which require high injection pressures. Moreover, all these studies focused only on melt flow in the filling process. Research concerning melt flow in the post-filling stage has yet to be reported. In view of this, the present researchers have proposed an alternative way of studying polymer melt flow in the injection molding process using the sequential injection capability of the coinjection molding machine.

In conventional injection molding which deals with a single polymer material, there are many previously reported investigations of both simulation and experimental work. Relevant reviews can be found in Isayev (1987) and Tucker (1989). Although a decade ago there were a few pioneering experiments with the sandwich injection molding process implemented with home-made equipment (Donovan et al., 1975; White and Lee, 1975; Young et al., 1980), research on the coinjection molding process almost ceased until recently, when the promising feature of this process was rediscovered by industry (Eckardt, 1985, 1986; Kreisher, 1990). Theoretical investigations concerning the coinjection molding process are also very limited. Numerical simulation using the concept of a residence time approach has been developed by Advanced CAE Technology (Turng and Wang, 1993; Peters et al., 1994) very recently. A method for particle tracing was described at the fountain flow region of the skin melt using a simplified model for gapwise velocity distribution and the residence time concept (Turng and Wang 1993; Manas-Zloczower et al., 1987). This particle-tracing approach can provide an approximate description of the flow field around the flow front and is useful for the curing-kinetics calculation in reactive injection molding. However, solving the residence time distribution for complex coinjection of molded parts is not straightforward, and the study of more sophisticated schemes is still in progress (Turng and Wang, 1993; Peters et al., 1994).

In this article, recent experimental work and simulation of polymer melt flow during the sequential injection molding process are both presented. Experimental work was carried out using a Battenfeld coinjection molding machine equipped with a microprocessor and a closed-loop control. The machine can provide various molding capabilities, as well as reliable molding experiments. Phenomena for the polymer melt flow in the filling stage, including the fountain flow effect, geometry factors such as edge effect and corner effect, as well as flow under contraction and expansion geometry, were identified. Characteristics of the polymer melt flow during the post-filling stage were also investigated. A numerical algorithm based on the concept of the control-volume/finite-element method employed within each gapwise layer and the dual-filling-parameter particle-tracing technique were implemented to simulate both the core and skin melt front advancements. Both simulated and experimental results are illustrated and discussed.

Experiments

One three-cavity mold, shown in Figure 2, was built to conduct the process studies. Cavity I consists of three regions with a thickness varying from 4 mm to 2 mm and back to 4 mm. It was designed to observe the fountain flow effect under abrupt contraction and expansion geometry. Cavity II consists of a block insert to form the weld line and to introduce the asymmetric melt flow conditions. The thickness variation is described in Figure 2. Cavity III is a line-gated plate with a uniform thickness of 2 mm. At the end of the sprue, the mold was designed with several valve inserts so that each of the three cavities can be injected individually or simultaneously. In the present experiment, each cavity was injection molded independently.

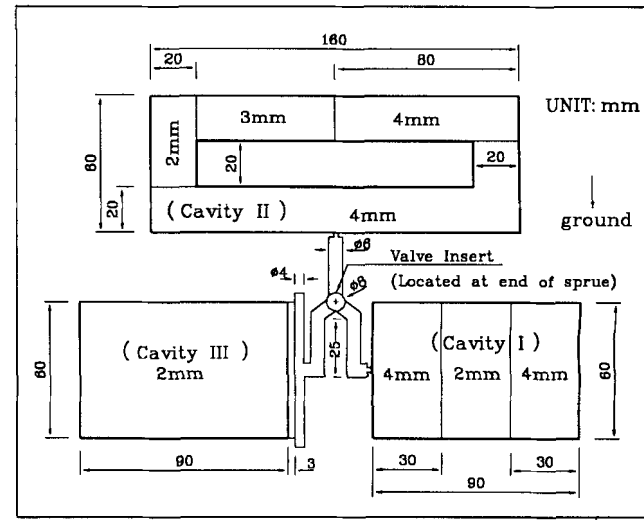

Figure 2. Geometry of the plate mold of three cavities.

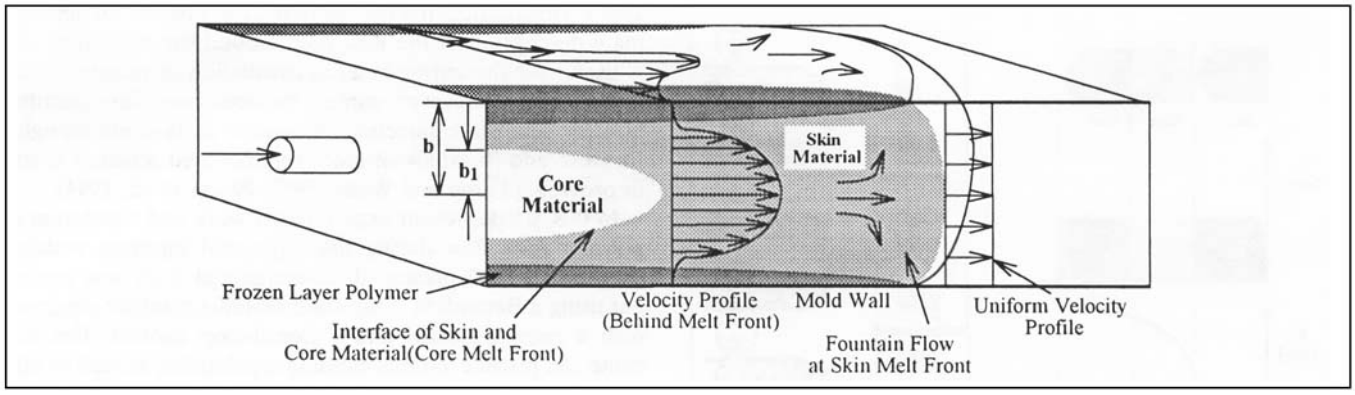

Figure 3. Skin and core melt fronts and skin-core interface in the cross-sectional view.

A 75-ton Battenfeld 750/750 coinjection molding machine was used for the present experiments. Transparent polystyrene (PS) resin was utilized as the skin material, whereas green-colored PS of the same batch was used as the core melt so that the final distribution of both materials could be seen easily by viewing the molded parts. The melt temperatures for both skin and core resin were 220°C or 230°C. The mold temperature was 60°C. The switchover in injection sequence from the skin melt to the core melt and the core melt back to the skin melt were varied according to the geometry of each mold cavity.

Process Formulation and Simulation

Formulation

It has been generally accepted that the Hele-Shaw type of flow model provides a reasonably accurate description of polymer melt flow in three-dimensional thin cavities. As a result, the relevant governing equations for the inelastic, non-Newtonian fluid flow under nonisothermal conditions are similar to those used in conventional injection molding (Hieber and Shen, 1980; Wang et al., 1986; Chen et al., 1988)

$$\frac{\partial P}{\partial x} = \frac{\partial}{\partial z}\left(\eta \frac{\partial u}{\partial z}\right) \tag{1}$$

$$\frac{\partial P}{\partial y} = \frac{\partial}{\partial z}\left(\eta \frac{\partial v}{\partial z}\right) \tag{2}$$

$$\frac{\partial}{\partial x}(b\bar{u}) + \frac{\partial}{\partial y}(b\bar{v}) = 0 \tag{3}$$

$$\rho C_p\left(\frac{\partial T}{\partial t} + u\frac{\partial T}{\partial x} + v\frac{\partial T}{\partial y}\right) = k\frac{\partial^2 T}{\partial z^2} + \eta\dot{\gamma}^2 \tag{4}$$

where P, T, u and v represent pressure, temperature and melt velocities in the x and y directions, respectively. The half thickness of mold cavity in the gapwise direction z is designated by b. Correspondingly, $\bar{u}$ and $\bar{v}$ designate gapwise averaged velocities for u and v. In addition, $\dot{\gamma}$, η, ρ, C_p and k represent shear rate, viscosity, density, specific heat, and thermal conductivity, respectively, for the polymer melt. The governing equations for the melt delivery system can also be written in a similar way in cylindrical coordinates. Details have been previously reported (Wang et al., 1986; Chen et al., 1988; Hsu, 1994). It is also assumed that a sharp interface exists between the skin and core materials, as depicted in Figure 3. Therefore, shear stresses and heat fluxes are continuous along the skin-core interface,

$$\left(\eta \frac{\partial u}{\partial z}\right)_{\text{skin}} = \left(\eta \frac{\partial u}{\partial z}\right)_{\text{core}} \tag{5}$$

$$\left(\eta \frac{\partial v}{\partial z}\right)_{\text{skin}} = \left(\eta \frac{\partial v}{\partial z}\right)_{\text{core}} \tag{6}$$

$$\left(k \frac{\partial T}{\partial z}\right)_{\text{skin}} = \left(k \frac{\partial T}{\partial z}\right)_{\text{core}} \tag{7}$$

The viscosity of the polymer melt is described by a modified-Cross model (Wang et al., 1986) with Arrhenius temperature dependence, that is,

$$\eta(T, \dot{\gamma}) = \frac{\eta_0(T, P)}{1 + (\eta_0 \dot{\gamma}/\tau^*)^{1-n}} \tag{8}$$

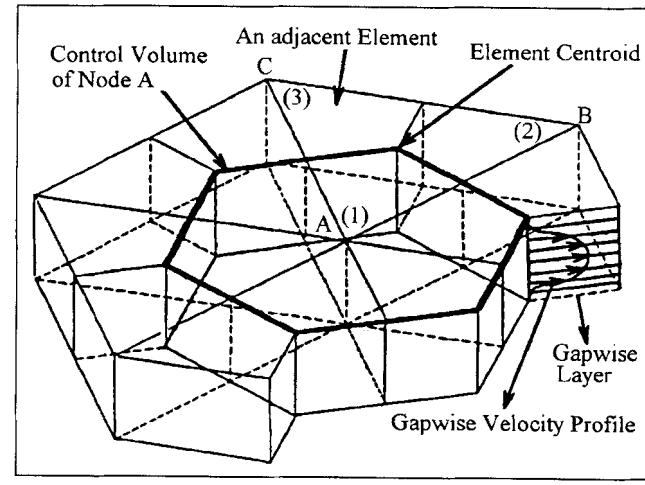

Figure 4. Control volume centered at node A.

Control volume is constructed by connecting the centroids of all the adjacent finite elements around node A.

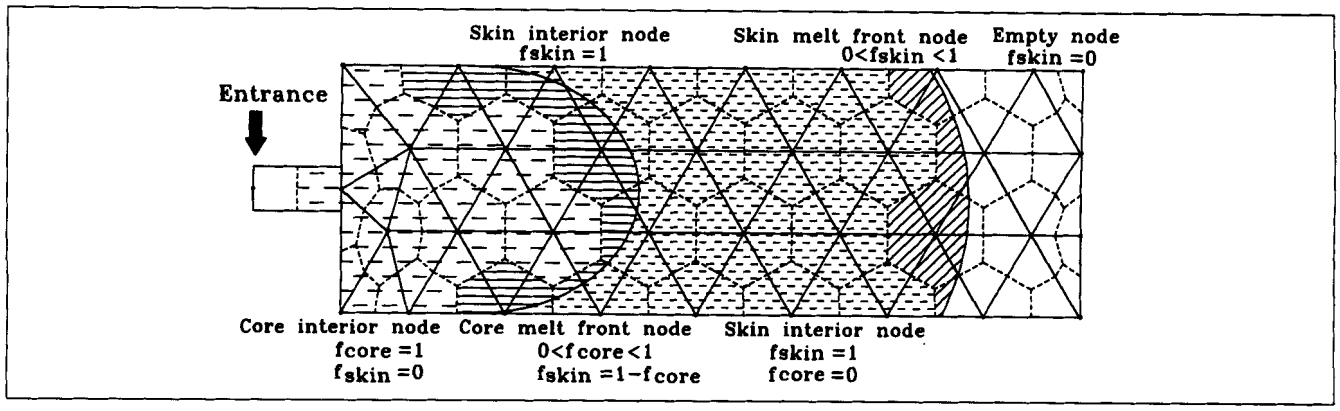

Figure 5. Dual filling parameters used to identify the skin and melt front locations at a specified layer in the thickness direction.

with

$$\eta_0(T,P) = B\exp\left(\frac{T_b}{T}\right)\exp(\beta P) \tag{9}$$

For polystyrene (CHI MEI/PG33), the material constants in the modified-Cross viscosity model are $n = 0.2838$, $\tau^* =$ 1.791E+04 Pa, $B = 2.591$E-07 Pa·s, $T_b = 11{,}680$ K, and β is taken to be zero assuming the small pressure dependence of viscosity. The density, specific heat, and thermal conductivity of PS are 940 kg/m^3, 2,100 J/kg·K, and 0.18 W/m·K, respectively. Density and specific heat were measured by the Material Research Laboratory of Industrial Technology & Research Institute following ASTM procedures, and thermal conductivity measurement follows procedures reported by Lobo and Cohen (1988).

Equations 1 and 2 can be combined with Eq. 3, making appropriate nonslip and symmetry boundary conditions, resulting in a governing equation for pressure

$$\frac{\partial}{\partial x}\left(S\frac{\partial P}{\partial x}\right) + \frac{\partial}{\partial y}\left(S\frac{\partial P}{\partial y}\right) = 0 \tag{10}$$

with S defined by

$$S + \int_0^{b_1}\frac{z^2}{\eta_{\text{core}}}\cdot dz + \int_{b_1}^{b}\frac{z^2}{\eta_{\text{skin}}}\cdot dz \tag{11}$$

where b_1 is the half thickness of the core melt in the gapwise direction and η_{core} and η_{skin} are viscosity values for the core and skin melts, respectively. S can be considered as the flow conductance or fluidity of the molten plastics. In the region where only skin melts exist, then $b_1 = 0$.

Numerical algorithm and simulations

For solving the pressure field during skin melt injection, Eq. 10 of the elliptic form is discretized using the standard Galerkin finite-element method. The control volume approach can also be employed directly to obtain the same discretized form (Wang et al., 1986; Chen et al., 1988; Hsu, 1994).

The net flow $q_i^{(\ell)}$ that enters the control volume centered at node A (see Figure 4) from an adjacent element ℓ, can be represented by

$$q_i^{(\ell)} = S^{(\ell)}\cdot\sum_{k=1}^{2\text{ or }3}\cdot D_{ik}^{(\ell)}\cdot P_k^{(\ell)} \tag{12}$$

where i is the local index for node A in the element ℓ and $i = 1$, 2, or 3 for triangular elements and $i = 1$ or 2 for rodlike elements. Subscript k denotes the local node index in element ℓ and $D_{ik}^{(\ell)}$ is the influence coefficient of the nodal pressure to the net flow in element ℓ. At the entrance, the net flows from all adjacent elements must satisfy the following relationship

$$\sum_{\ell'} q_i^{\ell'} = \frac{Q}{2} \tag{13}$$

where Q is the total volumetric flow rate of polymer melt. For the interior nodes, the net flows from all adjacent elements obey the conservation of mass law and are equal to zero, i.e.,

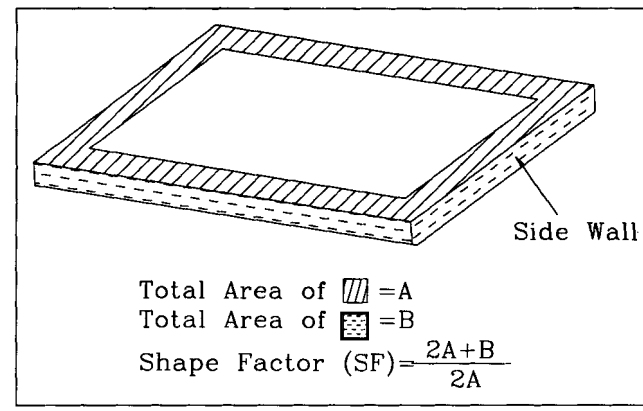

Figure 6. Definition of the shape factor used to correct the additional heat transfer caused by the side walls of the cavity.

Figure 7. Sequential injection of skin and core melts.

Skin melt was first injected for a 46.4% of the full injection stroke followed by a core melt injection of: (a) 28.6%, (b) 50% the full injection stroke. Finally, skin melt of the left stroke (a) (25%) and (b) (3.6%) was injected.

$$\sum_{\ell'} q_i^{\ell'} = 0 \tag{14}$$

At the melt-front nodes, the nodal pressures are equal to zero (gage pressure). To distinguish the entrance node and the interior nodes from the melt-front nodes, a filling parameter f_{skin} is defined and calculated during all analyses. For the entrance node and the interior nodes, f_{skin} is equal to 1, whereas $0 < f_{skin} < 1$ for melt-front nodes. When f_{skin} is 0, the node is designated as an empty node. This node definition is shown in Figure 5. At the melt-front nodes, the net flow entering the control volume from neighboring elements filled with melt can be computed. The analysis interval is chosen so that only one melt-front node gets filled per step (Wang et al., 1986; Chen et al., 1988). Once the pressure field is solved, the gapwise velocity profile and the associated shear rate values can be calculated. At the melt fronts, a uniform temperature profile and velocity profile of the gap average are usually assumed to account for the fountain flow effect in most simulation works, for example, in the reports by Krueger and Tadmor (1980) and Turng and Wang (1993).

When the core melt is injected into the cavity, the same algorithm employed for the node identification mentioned above can also be applied. However, the filling parameters now must be defined on each gapwise layer of the element with each divided into ten layers along the thickness direction. In addition, during the analysis of the core melt front advancement, it is necessary to identify the upstream nodes that are already filled with core melts. That is, among the

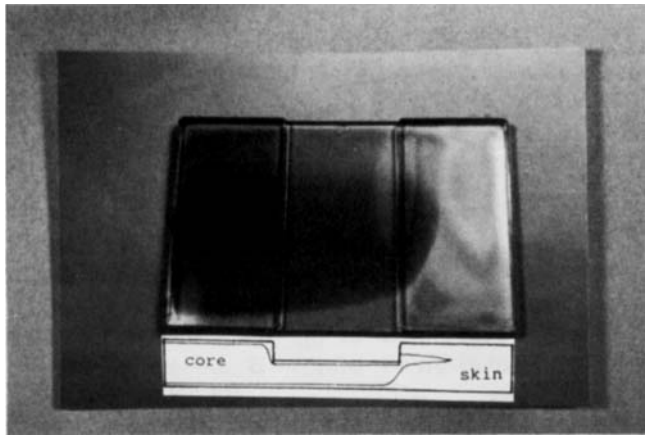

Figure 8. Core and skin melt material distribution when the melts flow through contraction and expansion geometry.

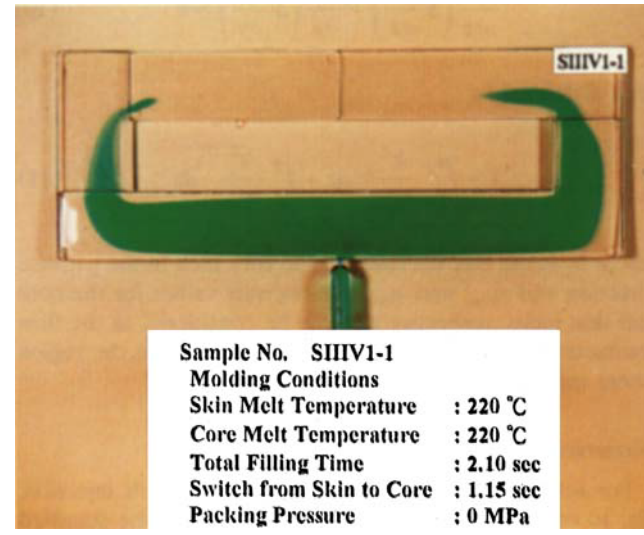

Figure 9. Sequential injection molded plate (cavity II) showing strong edge and corner effects.

Molding Conditions
Skin Melt Temperature : 230 °C
Core Melt Temperature : 230 °C
Total Filling Time : 1.31 sec
Skin to Core Switch Time : 0.60 sec
Core to Skin Switch Time : 0.45 sec
Packing Pressure : 0 Mpa

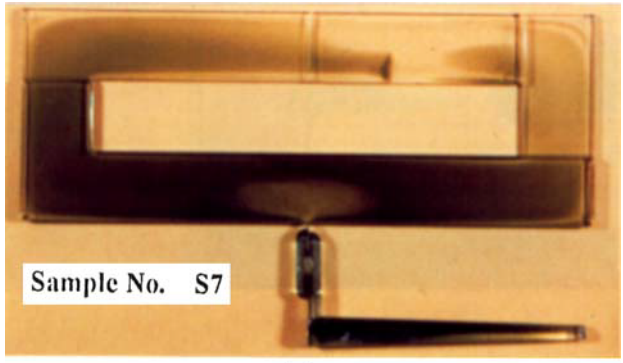

(a)

Molding Conditions
Skin Melt Temperature : 230 °C
Core Melt Temperature : 230 °C
Total Filling Time : 1.31 sec
Skin to Core Switch Time : 0.60 sec
Core to Skin Switch Time : 0.45 sec
Packing Pressure : 30 Mpa

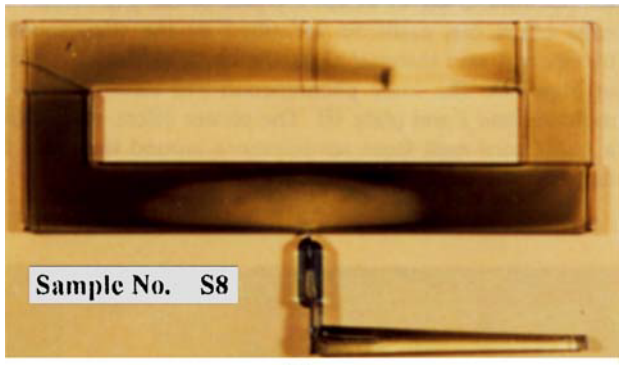

(b)

Molding Conditions
Skin Melt Temperature : 230 °C
Core Melt Temperature : 230 °C
Total Filling Time : 1.31 sec
Skin to Core Switch Time : 0.60 sec
Core to Skin Switch Time : 0.45 sec
Packing Pressure : 60 Mpa

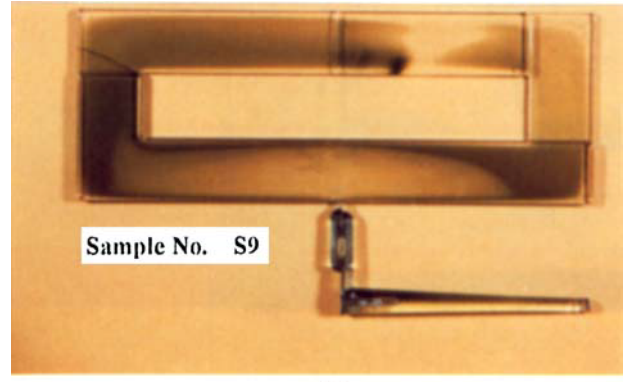

(c)

Figure 10.
Sequential injection molded part (cavity II):
(a) without applied packing pressure
(b) with applied packing pressure of 30 MPa
(c) with applied packing pressure of 60 MPa.

interior nodes filled with either melt, it is necessary to distinguish them by skin-only interior nodes, core melt-front nodes, and core-only interior nodes. This can be achieved by using the second filling parameter f_{core}. Dual filling parameters for the melt-front tracing technique is illustrated in Figure 5. The net flow rate that enters a control volume from an adjacent element ℓ in the jth layer can be obtained from the gapwise velocity profile defined at the centroid of the element ℓ (Figure 4). The analysis interval is chosen so that only one of the core melt-front nodes or the skin melt-front nodes on each gapwise layer becomes filled per analysis step (Wang et al., 1986; Chen et al., 1988).

In solving the temperature field, the same method reported previously by Wang et al. (1986) and Chen et al. (1988) is used. The calculation of nodal temperature is basically weighted from the subvolumes of all adjacent elements. However, the convection term considers only the contribution of the upstream elements. An implicit method is used for the conduction term, whereas the convection and viscous-heating terms were evaluated at the earlier step. The iteration criteria and algorithm are also similar to those in conventional injection moldings as reported by Wang et al. (1986) and Chen et al. (1988).

Since Hele-Shaw flow assumes a two-dimensional flow of infinite domain, the side walls of the mold cavity may introduce additional heat transfer and stresses during the polymer flow. To take the edge effect into account, shape factor values are used. The shape factor (SF) is calculated according to the ratio of the area for those mesh elements adjacent to the side walls plus the area of the side wall to the area of mesh

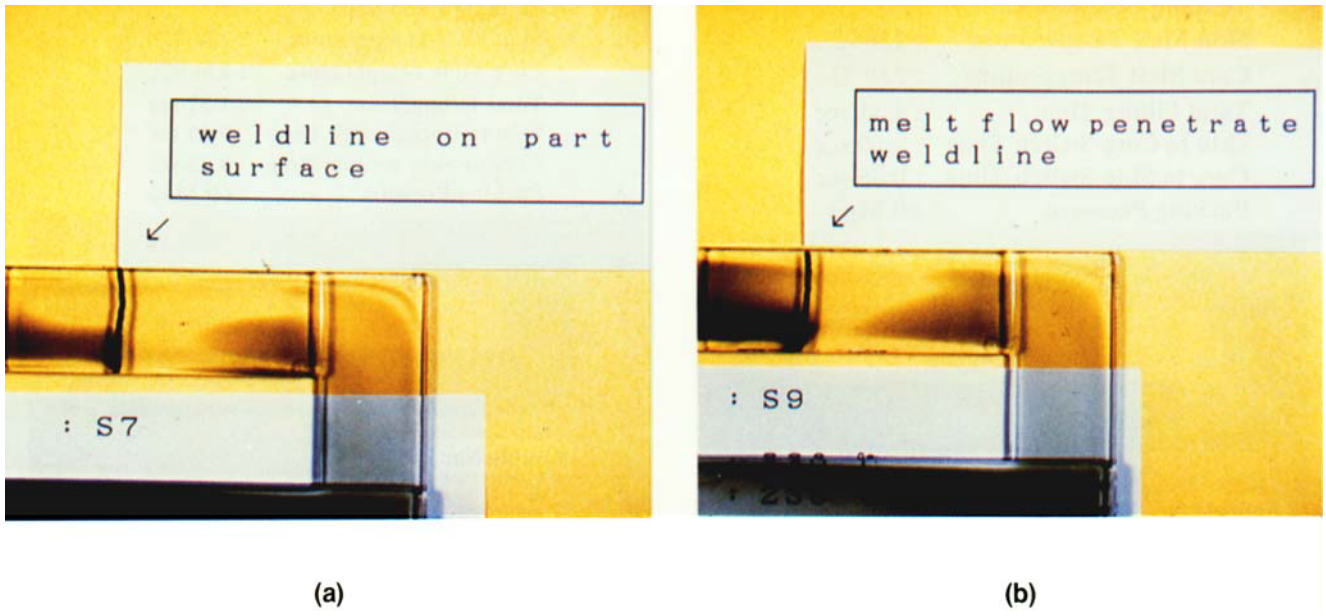

Figure 11. Enlarged view of the weld line area for sequential injection of the molded part (cavity II): (a) without applying packing pressure; (b) with applied packing pressure of 60 MPa.

elements adjacent to the side walls. The shape factor calculation is shown in Figure 6. Once the shape factor value is obtained, it can be combined with the thermal conductivity of the polymer melt to take the additional heat transfer from the side walls into account. The shape factor can also be combined with fluidity S. However, the physical meaning is not so straightforward.

Results and Discussion

Polymer melt flow in the filling stage

The fountain flow effect can be identified from the sequential injection molded plate of cavity III as shown in Figures 7a and 7b, respectively. In these two cases, transparent skin melt was injected first with a fixed stroke followed by the injection of green core melt with different strokes. It is evident that the core melt front is catching up with the skin melt front. Because of fountain flow effect, the velocity around the skin melt front is uniformly distributed in the gapwise direction and is smaller than the velocity of the core melt front located at the gap center of the cavity. As a result, the core melt front will advance faster than skin melt front once the core melt was injected. This phenomenon is also seen in all other experiments indicating that the fountain flow effect does exist and dominate the skin melt front movement. Although the fountain flow effect has been observed by other methods (Schmidt, 1974; Coyle et al., 1987; Vos et al., 1991), the present study provides an alternative method for observing the fountain flow effect. For the nonuniform thickness plate (cavity I), the asymmetric fountain flow of the core front in the gapwise direction was observed when flowing through the expansion juncture, as seen in Figure 8. Basically, the injected core melt will penetrate the hot core of skin melt through the gap center if the temperature on both cavity walls is the same. Under expansion geometry such as the juncture shown in Figure 8, the core melt front penetrates at a location slightly above the gap center. This indicates that when the skin melt flows through the expansion juncture, the melt temperature is higher at the top side of the gap center. The edge effect can easily be identified by the thin, solidified transparent skin material along the cavity side wall, as shown in Figure 9. The same phenomenon was also found in the molded plate I and plate III. The corner effect, which shows a faster core melt front advancement around the inner corner, was also clearly observed.

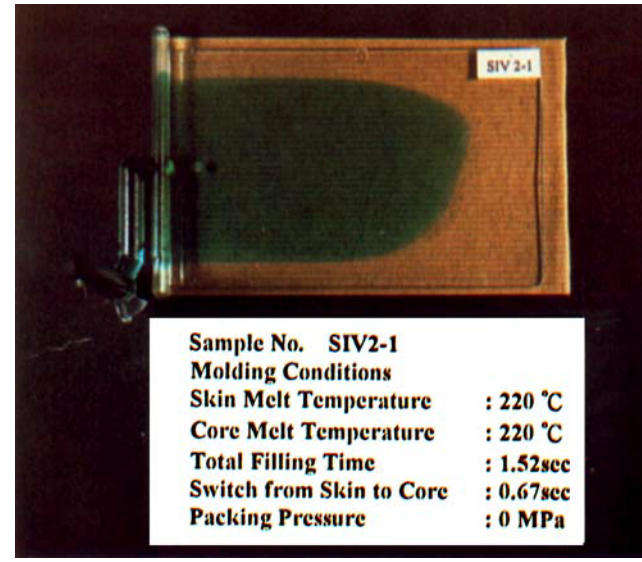

Figure 12. Experimental result showing core melt front location and core material distribution for the molded plate of cavity III.

Polymer melt flow in the post-filling stage

The sequential injection molded plates (cavity II) are shown in Figures 10a, 10b, and 10c, respectively, so that the polymer melt flow during the post-filling process may be observed. These parts are sequentially injected using a skin-core-skin sequence under different applied packing pressures. The injection sequence was designed so that the last injected transparent skin material barely enters the cavity. The applied packing pressures were set at 0 Mpa, 30 Mpa, and 60 Mpa, respectively. It was also clearly seen that the area of the transparent skin melt near the gate region increases as the packing pressure increases. It is evident that during the packing process additional polymer melt was pushed into the cavity due to the compressible nature of the melt. On the opposite side of the gate where the weld line was formed, the first injected skin melt and the core melt were also forced to flow as the packing pressure increased. However, the flows were less significant when compared with those near the gate location, as seen from the movement of the skin-core interface at the second skin melt front formed by the last skin melt injection. Interestingly, the melt flowed across the weld line around the gap center during the packing stage. The core melt front on the left side was located almost behind the weld line at the end of the filling process when no packing pressure was applied. If a 30 Mpa packing pressure was applied, the green core melt front moved to the location just beneath the weld line through the gap center where the melt temperature was still high. If a 60 Mpa packing pressure was employed, the core melt flowed farther ahead to cross the weld line slightly. The enlarged pictures are shown in Figures 11a and 11b, respectively.

Numerical simulation

Figure 12 shows one of the sequential injection molded plates of uniform thickness (cavity III) from which the final core melt front location, as well as the core material distribution, can be seen. Figure 13 shows the finite-element mesh used for the simulation. Based on this mesh, the calculated shape factor value is 1.2. Figure 14 represents the simulated results for the final core melt front locations at the gap center. The simulated location of the core melt front at the end of the filling stage is slightly behind the observed one. The consistency between the predicted value and the experimental data is reasonably good, indicating that the present numerical scheme is an acceptable method for the simulation of sequential injection molding. In addition, simulation using the present particle-tracing scheme is not subject to limitations of geometrical complexity as compared with that of the residence time approach which requires a simplified modeling of the flow field around the fountain flow region. The latter method is also difficult to apply to the post-filling stage when the mold cavity is filled. However, if the core melt breaks though the skin melt and flows to the part surface, the present scheme cannot be applied.

Finally, the edge effect is taken into account using the shape factor as a geometrical correction. The corresponding shape factor values are calculated and employed to measure the additional heat transfer from the side walls of the mold cavity. The corrections result in a more accurate core melt front location than that obtained without the geometrical correction. The situation is depicted in Figure 15. The simulation accu-

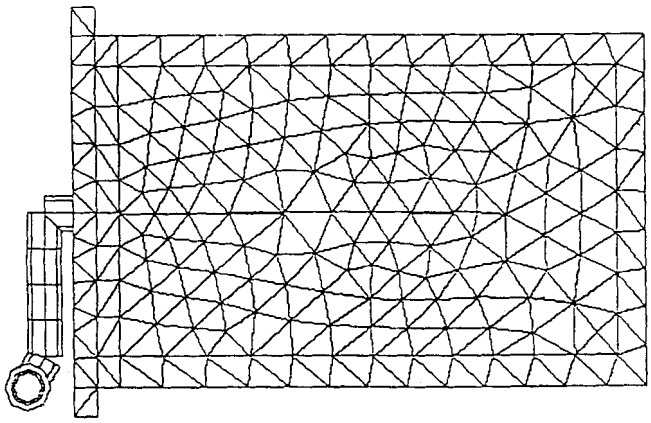

Figure 13. Finite-element mesh used for the simulation of cavity III.

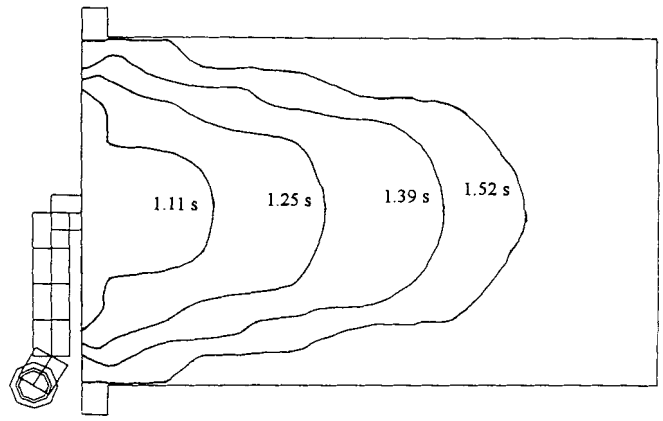

Figure 14. Simulated result for the core melt front advancement in the middle plane of the cavity gap for plate III without using the shape factor as a correction.

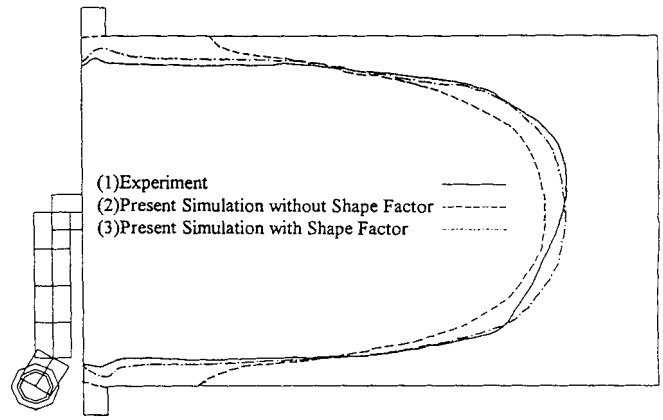

Figure 15. Comparison of simulated predictions and experimental results on the final core material distribution for plate IV.

Simulated results both with and without using shape factor correction are illustrated.

racy is further improved using the shape factor correction. However, since shape factor value is mesh-size dependent, more systematic studies are required.

Conclusions

Experimental studies of the polymer melt flow in mold filling and post-filling stages of the injection molding process were implemented using the sequential injection of transparent and colored polystyrene resin. In the filling stage the fountain flow effect, geometrical factors such as the edge effect, the corner effect, as well as flow through contractions and expansions were well identified. In the post-filling process, significant polymer melt flow which increases with increased packing pressure was observed. However, melt flows more significantly around the gate area than away from the gate. In addition, it was found that polymer melt flows across the gap center resulting in partial annihilation of the weld line. Simulations based on the control-volume/finite-element method employed within each gapwise layer combined with the dual-filling-parameter technique were developed to trace the melt front advancements for both skin and core materials. Numerical simulations show reasonably good consistency with experimental results in both skin and core material distribution. However, if the edge effect is taken into account using shape factor as a geometrical correction, the simulation accuracy can be further improved.

Acknowledgment

This work was supported by the National Science Council under NSC grant 83-0405-E033-027 and special group-research funding under the Computer Integrated Manufacture of Injection Molding Process Program of Chung Yuan University.

Notation

x = planar direction
y = planar direction
η_0 = viscosity constant, Eq. 8

Subscript

j = designation of gapwise layer index

Literature Cited

Chen, S. C., P. Pai, and C. Hsu, "A Study of Finite Element Mold Filling Analysis in Application," *SPE Tech. Papers*, **34**, 250 (1988).

Coyle, D. J., J. W. Blake, and C. W. Macosko, "The Kinematics of Fountain Flow in Mold-Filling," *AIChE J.*, **33**, 1168 (1987).

Donovan, R. C., K. S. Rabe, W. K. Mammel, and H. A. Load, "Recycling Plastics by Two-shot Molding," *Poly. Eng. Sci.*, **15**, 774 (1975).

Eckardt, H., "One-Step Production of Screened Housing with Good Surface Quality Made Possible by Two-component Injection Molding," *Kunststoffe*, **75**, 145 (1985).

Eckardt, H., "How to Develop a Successful Coinjection Application," *Proc. Structural Foam Conf.*, Soc. of Plastics Ind., Boston, p. 24 (Apr. 21–23, 1986).

Escales, E., "The ICI Sandwich Molding Process," *Kunststoffe*, **60**, 847 (1970).

Garcia, M. A., "Molding of Reactive Filling in Complex Cavities," *Int. Poly. Proc.*, **6**, 73 (1991).

Hieber, C. A., and S. F. Shen, "A Finite-Element/Finite-Difference Simulation of the Injection-Molding Filling Process," *J. Non-Newtonian Fluid Mech.*, **7**, 1 (1980).

Hsu, K. F., "Numerical Simulations of Multi-Component Injection Molding Process," Masters Thesis, Chung Yuan Univ., Taiwan (June, 1994).

Isayev, A. I., ed., *Injection and Compression Molding Fundamentals*, Marcel Dekker, New York (1987).

Kreisher, K. R., "Coinjection Molding Is Hot Again—With a Lot More Going for It," *Modern Plastics Int.*, 56 (Mar. 1990).

Krueger, W. L., and Z. Tadmor, "Injection Molding into a Rectangular Cavity with Inserts," *Poly. Eng. Sci.*, **20**, 426 (1980).

Lobo, H., and C. Cohen, "Measurement of Thermal Conductivity of Polymer Melt by the Line Source Method," *SPE Tech. Papers*, **34**, 609 (1988).

Manas-Zloczower, I., J. L. Blake, and C. W. Macosko, "Space-Time Distribution in Filling a Mold," *Poly. Eng. Sci.*, **27**, 1229 (1987).

Peters, G. W. M., P. J. L. van der Velden, and H. E. H. Meijer, "Multilayer Injection Molding Part 2: Particle Tracking in Reactive Moulding," *Int. Poly. Proc.*, **9**, 258 (1994).

Schmidt, L. R., "A Special Mold and Tracer Technique for Studying Shear and Extensional Flows in a Mold Cavity During Injection Molding," *Poly. Eng. Sci.*, **14**, 797 (1974).

Tucker, C. L., ed., *Fundamentals of Computer Modeling for Polymer Processing*, Hanser Publisher, New York (1989).

Turng, L. S., and K. K. Wang, "Numerical Simulation of the Coinjection Molding Process," *ASME, J. Eng. Mat. & Tech.*, **115**, 48 (1993).

Vos, E., H. E. H. Meijer, and G. W. M. Peters, "Multilayer Injection Molding," *Int. Poly. Proc.*, **6**, 42 (1991).

Wang, V. W., C. A. Hieber, and K. K. Wang, "Dynamic Simulation and Graphics for the Injection Molding of Three-Dimensional Thin Parts," *J. Poly. Eng.*, **7**, 21 (1986).

White, J. L., and B. L. Lee, "An Experimental Study of Sandwich Injection of Two Polymer Melts Using Simultaneous Injection," *Poly. Eng. Sci.*, **15**, 481 (1975).

Yokoi, Y., S. Kamata, and T. Kanematsu, "Visual Observation of Three-Dimensional Melt Flow Inside a Mold Cavity by Gate-Magnetization Method," *SPE Tech. Papers*, **37**, 358 (1991).

Yokoi, Y., Y. Murata, and K. Oka, "Visual Analysis of Weld Line Vanishing Process by Glass-Insert Mold," *SPE Tech. Papers*, **37**, 367 (1991).

Yokoi, Y., and Y. Inagaki, "Dynamic Visualization of Cavity Filling Process along Thickness Direction Using a Laser-Light-Sheet Technique," *SPE Tech. Papers*, **38**, 457 (1992).

Young, S. S., J. L. White, E. S. Clark, and Y. Oyanagi, "A Basic Experimental Study of Sandwich Injection Molding with Sequential Injection," *Poly. Eng. Sci.*, **20**, 798 (1980).

Manuscript received Nov. 10, 1994, and revision received Aug. 31, 1995.